Biomedical Physics & Engineering Express

PAPER

A model based investigation of the period doubling behavior in human steady-state visual evoked potentials

RECEIVED
11 April 2019

REVISED
18 June 2019

ACCEPTED FOR PUBLICATION
26 June 2019

PUBLISHED
11 July 2019

Yiğit Tuncel, Toygun Başaklar and Yusuf Ziya Ider[1]

Electrical and Electronics Engineering Department, Bilkent University, Ankara, Turkey
[1] Author to whom any correspondence should be addressed.

E-mail: yttuncel@asu.edu, basaklar@ee.bilkent.edu.tr and ider@ee.bilkent.edu.tr

Keywords: EEG, steady state visual evoked potential, SSVEP, cortex models, corticothalamic model, subharmonic, period doubling

Abstract

Objective. This study aims at investigating the potential mechanism of period doubling (PD) (subharmonic generation) in human steady-state visual evoked potentials (SSVEPs) by using a mathematical model. *Approach.* Robinson's Corticothalamic Model, which includes three main neuronal populations (cortical, thalamic reticular, and thalamic relay neurons) was employed. SSVEP experiments were simulated using this model and dependence of PD behavior in relation to the values of model parameters was investigated. The feedback loop in the model that is responsible for the generation of subharmonic components was thus identified, and this loop was isolated from the rest of the model and analyzed with a describing function approach. *Main Results.* It has been found in general, for a wide range of parameter values, that if the excitation frequency or half of it is close to the native oscillation frequency of the system, the native oscillation ceases to exist and oscillations at either the excitation frequency or half of it are observed. This observation is in line with the experimental findings except for some discrepancies which are also discussed. The intrathalamic feedback loop is identified to be the potential source of subharmonic oscillations. When isolated from the rest of the model and simulated by itself, it has been found that this feedback loop can show a resonance phenomenon at the subharmonic frequency. By deriving a set of equations based on the necessary conditions for a resonance phenomenon, a semi-analytical method was developed by which one can predict the existence of subharmonic generation for a given set of parameters and stimulus frequency. *Significance.* This study is the first model-based investigation of the mechanism of subharmonic oscillations. The proposed semi-analytical method can replace extensive time and memory consuming parameter sweep studies.

1. Introduction

Steady-State Visual Evoked Potentials (SSVEPs) are oscillatory brain potentials elicited in the electroencephalogram (EEG) in response to periodic light stimulation [1–5]. These responses are characterized as oscillations at the stimulus frequency as well as its harmonics and subharmonics [2, 6, 7]. Particular interest has been shown to understanding some of the nonlinear dynamics of the SSVEP responses, including harmonics generation, alpha entrainment to stimulus frequency and frequency mixing [2, 6, 8–12]. The generation of subharmonics, on the other hand, has not received much attention.

We refer to the generation of the first subharmonic component as Period Doubling (PD) Phenomenon, i.e. given a flickering stimulus with a frequency of f, we observe a strong and distinct component at $f/2$ in the EEG spectrum. This phenomenon has been observed in several experimental SSVEP studies for different frequency ranges. Herrmann's findings indicated that subharmonic generation may occur for stimulation frequencies in 15–30 Hz range [6]. Crevier and Meister reported subharmonic components for stimulus frequencies between 30–70 Hz [13]. Tsoneva *et al* have observed subharmonic generation in the 40–60 Hz stimulus frequency range [14]. In addition to these studies, in our previous work, our results showed subharmonic generation for the stimulus range of 15–42 Hz [15].

Despite many years of research in this field, mechanisms that explain the nonlinear characteristics

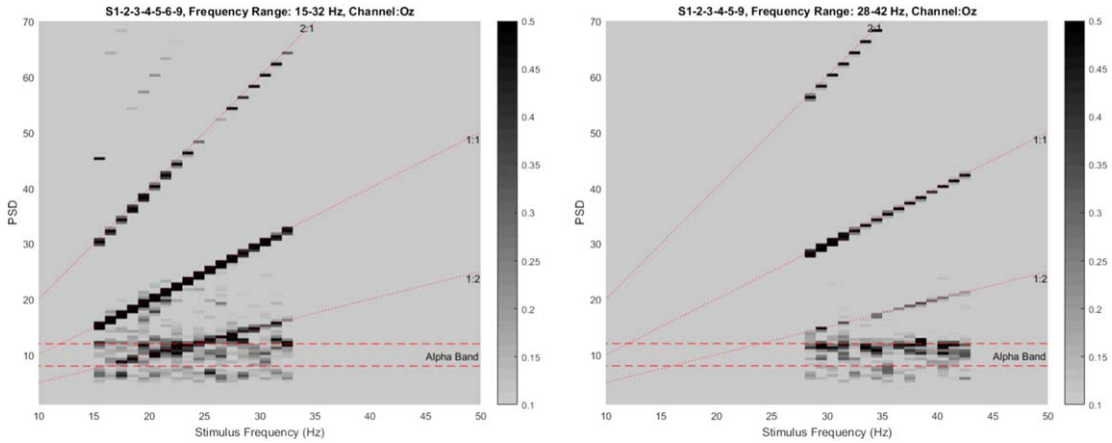

Figure 1. Averaged two dimensional plots across all subjects (Channel Oz) for the experiments in [15]. In these plots, the stimulation frequencies are placed on the horizontal axis and the PSD estimate of the response to each stimulus frequency is grayscale coded on the vertical axis. The left plot covers the stimulus frequencies from 15 Hz to 32 Hz and the right plot covers the stimulus frequencies from 28 Hz to 42 Hz. Horizontal dashed red lines visualize the alpha band (8–12 Hz interval). The dotted red lines are put for better demonstration of the trends in data. The lower limit of the colorbar is set to 0.1 to eliminate confusion due to background noise in spectrums. The upper limit is saturated at 0.5 for clear observation of subharmonic peaks.

of the SSVEP responses are still unresolved [8]. In more recent years, modelling studies have started to emerge [16–18], that aim to explore and analyze such mechanisms.

Spiegler *et al* have investigated [18] the photic driving effect (i.e. frequency entrainment) of a periodic light stimulus through a modified Zetterberg-Jansen model [19]. They drove the model with a rhythmic input consisting of a train of pulses where each pulse is similar to that used by Jansen and Rit [19]. They demonstrated many different nonlinear dynamics the model can produce, including chaos. Particularly, they investigated the effect of stimulus amplitude on the entrainment phenomenon and came up with various predictions. In this work, however, authors did not mention any subharmonics generated by the cortical model.

Robinson's Corticothalamic Model, which has been shown to successfully predict various phenomena in the EEG, has been driven by Roberts and Robinson with periodic input [17, 20–22]. They tested the model against Herrmann's experimental findings [6] and observed subharmonic components at the model output for stimulus frequencies in the 15–24 Hz interval which coincides with the experimental results. They have stated that alpha oscillations entrain to the stimulation frequency or its first subharmonic if either of these fall in the alpha range. However, they have not discussed how and where in the model such behavior is generated.

Labecki *et al* have driven the neural mass model of Lopes da Silva *et al* [23] also with periodic input [16]. They observed subharmonic responses in the model output for stimulus frequencies (for sine wave input) between 17–21.5 Hz. They also showed that for subharmonic oscillations to occur, a feedback loop with at least one nonlinear element is necessary in the mathematical model.

Considering all the previous work, one might argue that subharmonic components in SSVEP responses could be a focus of new experimental and theoretical studies. In this work, we aim to understand using a mathematical model where and how in the visual system such subharmonic components emerge. For this purpose, we employ Robinson's Corticothalamic Model, analyze its PD behavior in response to a sinusoidal drive under different parameter configurations and also compare its predictions with our experimental findings [15]. We have identified the intrathalamic feedback loop of the model as the possible source of subharmonic components. Additionally, we have investigated, by nonlinear feedback theory, the possible generation mechanism of subharmonic oscillations in this feedback loop.

2. Materials and methods

2.1. Experimental data

The experimental data which is referred to and discussed in this study has been published in [15]. A brief explanation of the experimental procedure is given in appendix A and figure 1 shows the experimentally obtained power spectral density (PSD) versus stimulation frequency plots.

2.2. Computational model

In this work, we use a neural field model that had been proposed by Robinson *et al* to model cortico-thalamic dynamics [20–22]. This model includes three main neuronal populations, cortical neurons (excitatory (e) and inhibitory (i) interneurons and implicitly pyramidal cells), thalamic reticular (r) neurons and thalamic

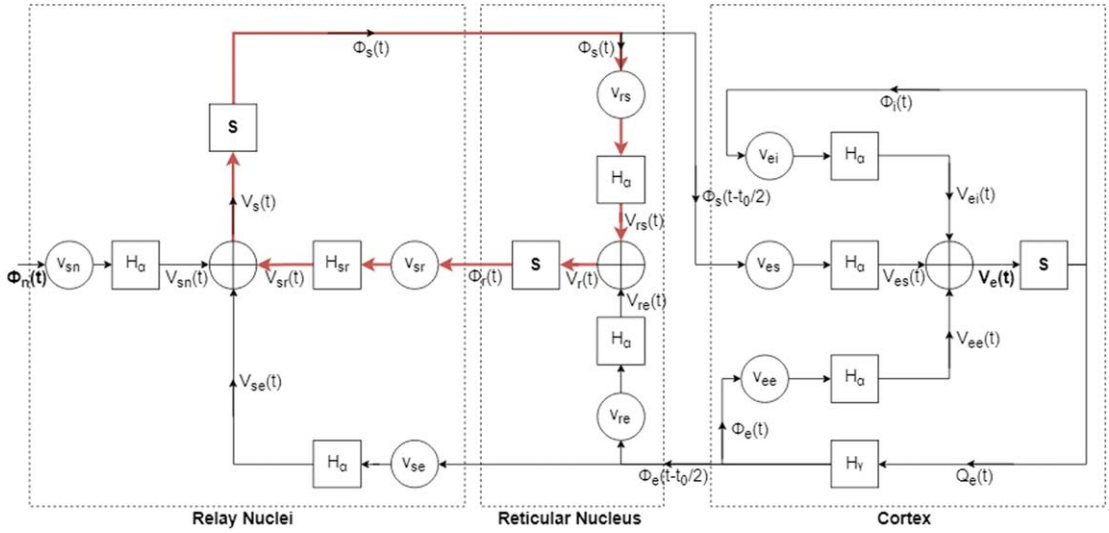

Figure 2. Representation of Robinson's Corticothalamic Model as a block diagram. There are three main populations in the model: (i) Relay Nuclei (ii) Reticular Nucleus (iii) Cortex. Their contents are marked with dashed boxes. There are three types of blocks in the whole model: (i) gain blocks denoted with v_{ab} (ii) second order transfer functions denoted with H (iii) sigmoidal type nonlinear blocks denoted with S. Input to the model is given via ϕ_n while the output is taken from V_e. Notice the red highlighted intrathalamic loop from which subharmonic oscillations seem to arise.

relay (s) neurons. In our experiments [15], we have used a full visual field stimulus. This allows us to assume spatially uniform stimulation of the visual cortex, hence allowing us to model the entire visual cortex with a single neuronal population. With such assumption, we also omit the spatial dependence of the model and thus reduce it to a neural mass model. The explanation and formulation of model differential equations are given in appendix B.

For the sake of easier analysis and modification of the model equations, we also implemented the model in Simulink (The MathWorks, Inc., Natick, MA, USA) environment. For this purpose, differential operators D_α, D_{sr} and D_γ (see App. B) are converted to transfer functions of the following forms:

$$D_\alpha \rightarrow H_\alpha(s) = \frac{\alpha\beta}{s^2 + (\alpha+\beta)s + \alpha\beta}$$
$$D_{sr} \rightarrow H_{sr}(s) = \frac{\alpha_{sr}\beta_{sr}}{s^2 + (\alpha_{sr}+\beta_{sr})s + \alpha_{sr}\beta_{sr}}$$
$$D_\gamma \rightarrow H_\gamma(s) = \frac{\gamma^2}{s^2 + 2\gamma s + \gamma^2} \quad (1)$$

The model can be expressed as a block diagram as in figure 2. Here, when the cortical circuit is examined, one can interpret that pyramidal cell population is in fact explicitly modeled and the interneuron populations are implicitly modeled through synaptic strengths v_{ei} and v_{ee}. That is to say, output of the pyramidal cell population $S[V_e(t)]$ is scaled by gains v_{ei} and v_{ee} and then converted to contributions to mean soma potential of the pyramidal cell population (V_{ei} and V_{ee}). Hence, we adopt V_e as the main source of the recorded scalp EEG which is thought to correspond to the mean membrane potential of the pyramidal cell population [24]. Simulink is set to solve the model with a forward Euler integration scheme with $dt = 10^{-4}$ s.

Since lateral geniculate nucleus of the thalamus acts as the relay station for sensory inputs coming to the brain [21] (hence the name relay nucleus in the model), input to the model (ϕ_n) is given via the relay nucleus. We model the input as background activity and stimulus superimposed:

$$\phi_n(t) = \phi_n^{BG} + \phi_n^{stim}$$

Here, ϕ_n^{BG} denotes the background activity. Generally, this activity is modeled as a DC plus a zero-mean Gaussian white noise. However, we believe the stimulus in our experiments would dominate the amount of noise in the background activity, so we only consider ϕ_n^{BG} as a constant value. ϕ_n^{stim} is simply a cosine at the stimulation frequency with amplitude Φ_n. In doing this, we make the assumption of ignoring the potential role of retinal dynamics in the experimentally observed PD phenomenon.

In earlier studies of this model, different values (or ranges) for model parameters were discussed [17, 21, 25, 26]. In this study, these ranges were taken into consideration during parameter assignments. In their 2012 study [17], Roberts and Robinson drove this model with a sinusoidal input and shared a parameter set that would better resemble the features and trends in the experimental data of Herrmann [6]. In this work, we took their parameter set as the starting point in our model analysis (i.e. as the default parameter set). We also undertook rather limited parameter sweep studies in which we considered the parameter ranges mentioned in the literature. We refrained from doing an extensive parameter sweep study, because with such a high order model (17 parameters) doing such a

Table 1. The parameter set that we used to run the model and initially make our observations from. These values are taken from [17] where the authors drove this model with a sinusoidal input and shared a parameter set that would better resemble the features and trends in the experimental data of Herrmann [6].

$\nu_{se} = 2.9$, $\nu_{sr} = -0.57$, $\nu_{re} = 0.67$, $\nu_{rs} = 2.9$, $\nu_{sn} = 1$, $\nu_{ee} = 1.3$, $\nu_{ei} = -2.9$, $\nu_{es} = 0.13$
$\alpha = 80s^{-1}$, $\beta = 800s^{-1}$, $\alpha_{sr} = 10s^{-1}$, $\beta_{sr} = 60s^{-1}$, $\gamma_e = 100$ $Q_{\max} = 250$, $\sigma = 3.3$, $\theta = 15$ $\phi_n^{BG} = 18$, $\phi_n^{stim} = 2.8$

work requires substantial amount of computational power and time.

2.3. Describing function

A conventional way of analyzing the transfer characteristics of nonlinear components in nonlinear feedback systems is describing function (DF) analysis. The DF in this context, relates the amplitudes and phases of the components in the output of the nonlinearity to those of the components in its input. For polynomial type nonlinearities, describing functions can be analytically found [27, 28] but in our case the nonlinearity is a shifted sigmoid. Also, utilizing describing function analysis requires the linear part of the system to behave as a sharp low pass filter that completely filters out higher order components. However, for many values of the reciprocal time constants β and α (and others), this may not be the case in the model. Therefore, we have adopted Fourier Transform method to find the DFs. In this method, DFs are numerically computed by finding the Fourier coefficients in its output in relation to the input [28]. Calculating DFs for the nonlinearities allows us to write loop equations and solve these for amplitudes and phases of the oscillations in the system output by utilizing a numerical nonlinear system solver (fsolve in Matlab).

3. Results

3.1. Period doubling behavior in robinson's corticothalamic model with default parameters

We first reproduced the results of Roberts and Robinson's study [17]. The default parameters used are given in table 1:

A two dimensional plot similar to which was used to visualize experimental results was formed from the model responses to stimulation frequencies in the 1–50 Hz interval (figure 3). It can be seen that alpha band power is concentrated at $f_\alpha = \sim$11 Hz (model's native oscillation frequency). Here it is obvious that, when driven with a sinusoidal input with an amplitude $\phi_n^{stim} = 2.8$ and bias $\phi_n^{BG} = 18$, the model can generate subharmonics in the 15–25 Hz stimulus frequency region. We have also made the following observations (as also conjectured by Roberts and Robinson [17] regarding entrainment): from 0–5 Hz we observe the natural oscillation of the system (alpha oscillation) which is around $f_\alpha = 11$ Hz. Between 6–14 Hz, it appears that the native oscillation entrains to the excitation frequency. Between 15–25 Hz, the native oscillation entrains to half of the excitation frequency. Therefore, roughly speaking, 6–14 Hz range is the entrainment range in the sense that the native oscillation shifts to the excitation frequency or half of it whichever falls in this range.

3.2. Identification of the source of PD generation within the Robinson's corticothalamic model

We modified the gains of some feedback loops as follows: (i) we cut off cortical feedback connection by setting ν_{re} and ν_{se} (both separately and together) to zero, or (ii) we cut off intrathalamic feedback connection by setting ν_{rs} and ν_{sr} (both separately and together) to zero, and observed thalamic and cortical outputs ϕ_s and ϕ_e respectively. We found out that regardless of whether the cortical feedback connections (ν_{re} and ν_{se}) are cut off or not, there is subharmonic generation at both outputs as long as the intrathalamic loop is maintained. This loop is highlighted in red in figure 2. Therefore, we argued that these subharmonic oscillations are generated in the intrathalamic feedback loop. As we experimented with the gains of the feedback loops, we also observed how the native oscillatory behavior of the system (alpha rhythm) is affected. By setting ν_{sr}, ν_{re}, ν_{se} to zero, the alpha oscillation is not observed indicating that the cortex is by itself not sufficient to generate the alpha rhythm. Interestingly, in the absence of an intrathalamic feedback loop ($\nu_{rs} = 0$ and/or $\nu_{sr} = 0$), the alpha rhythm at the system output vanishes. Furthermore, when ν_{re} and ν_{se} are taken as zero, alpha oscillation is still observed. All these suggest that the alpha oscillation is also generated in the aforesaid intrathalamic loop.

3.3. Determination of the parameters that affect PD behavior

We then focused on the effects of different parameters of the intrathalamic feedback loop to subharmonic generation. The parameters in this loop are ν_{sr}, ν_{rs}, ν_{sn}, α, β, α_{sr}, β_{sr}, $Q_{\max}$, σ, θ, ϕ_n^{BG} and ϕ_n^{stim}. We neglected ν_{sn} as the same effect would be observable when ϕ_n^{stim} and ϕ_n^{BG} are varied instead, so we are left with 11 parameters. We used a coarse grid (4 to 10 values per parameter) for the parameter spaces for the sake of simplicity. While values for a parameter is being swept, other remaining parameters are set to default values (table 1).

In figure 4, effects of four parameters (ϕ_n^{stim}, α, α_{sr}, ϕ_n^{BG}) on subharmonic generation is shown. The effects of the remaining 7 parameters are given in appendix C. From these four parameters, ϕ_n^{stim} had been previously investigated in [17]. Same results are again visible in figure 4. In this case, ϕ_n^{stim} is increased from 1 to 5. When it is set to 1, the subharmonic generation seems to occur at stimulation

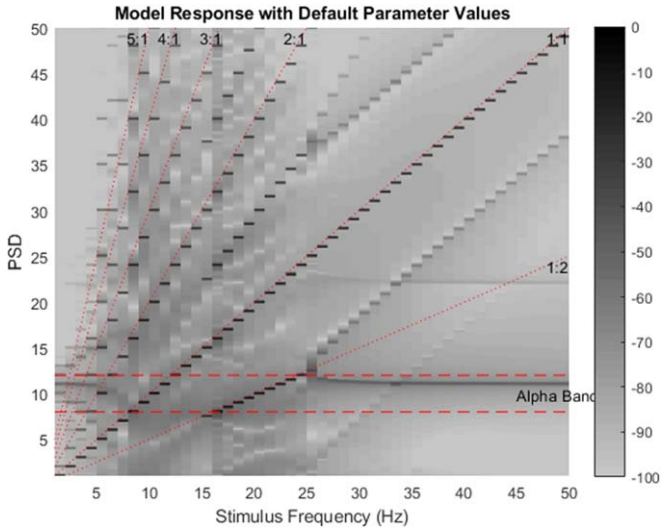

Figure 3. The two dimensional plot of the model responses to stimulation frequencies from 1 to 50 Hz with parameter values chosen as in table 1. In this plot, the stimulation frequencies are placed on the horizontal axis and the PSD estimate of the response to each stimulus frequency is grayscale coded on the vertical axis. Notice that unlike the experimental plots (figure 1), this plot is in logarithmic scale. It can be seen that the alpha band component is being entrained to fundamental components (1:1 line) in frequencies between 6–14 Hz, and then to subharmonic components (1:2 line) in frequencies between 15–25 Hz. At other frequencies (0–5 Hz and 25–50 Hz) the power at alpha frequency (~11 Hz) can be seen as a horizontal gray line.

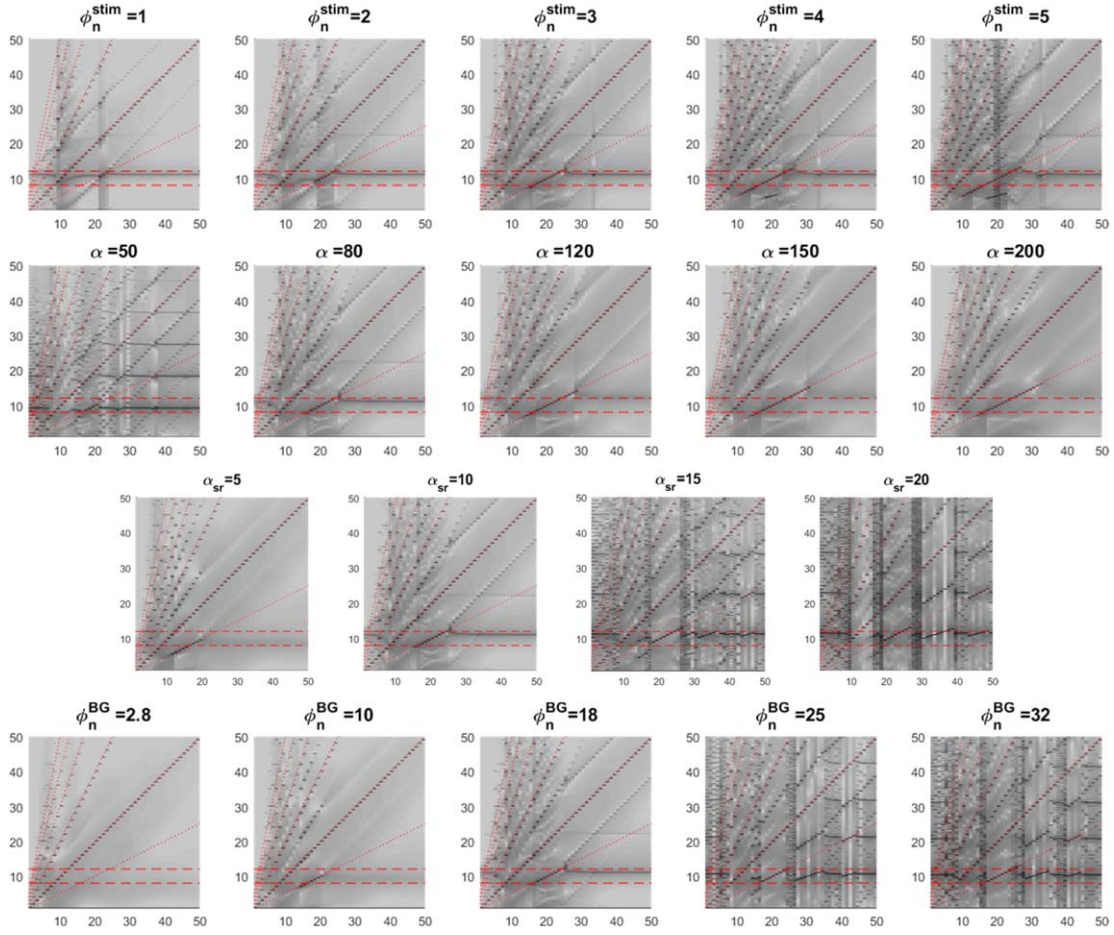

Figure 4. Effects of four parameters (α, α_{sr}, ϕ_n^{stim}, ϕ_n^{BG}) on subharmonic generation. In these plots, the stimulation frequencies are placed on the horizontal axis and the PSD estimate of the response to each stimulus frequency is grayscale coded on the vertical axis. Topmost row shows model responses for $\phi_n^{stim} = 1, 2, 3, 4, 5$, second row for $\alpha = 50, 80, 120, 150, 200$, third row for $\alpha_{sr} = 5, 10, 15, 20$, and bottommost row for $\phi_n^{BG} = 2.8, 10, 18, 25, 32$. While these values are swept for the relevant parameter, the values for other parameters are selected as in table 1.

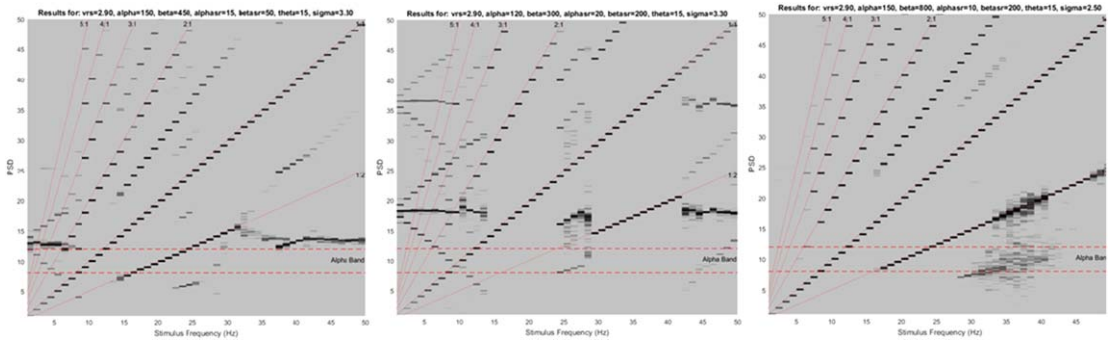

Figure 5. Model responses with very different subharmonic generation intervals for different parameter sets. In these plots, the stimulation frequencies are placed on the horizontal axis and the PSD estimate of the response to each stimulus frequency is grayscale coded on the vertical axis. Parameters are set as follows (values for the remaining parameters are selected as in table 1): In the leftmost plot $\alpha = 150$, $\beta = 450$, $\alpha_{sr} = 15$, $\beta_{sr} = 50$, $\theta = 15$, $\sigma = 3.3$, in the middle plot $\alpha = 120$, $\beta = 300$, $\alpha_{sr} = 20$, $\beta_{sr} = 200$, $\theta = 15$, $\sigma = 3.3$ and in the rightmost plot $\alpha = 150$, $\beta = 800$, $\alpha_{sr} = 10$, $\beta_{sr} = 200$, $\theta = 15$, $\sigma = 2.5$.

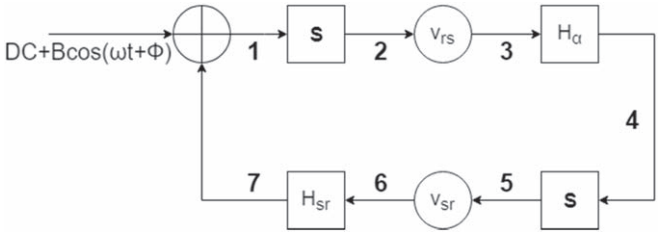

Figure 6. The isolated intrathalamic loop consists of two nonlinear elements (**S**), two gain elements (v_{rs} and v_{sr}) and two second order low pass filters (H_a and H_{sr}). The loop is driven with a signal of the form $DC + Bcos(\omega t + \phi)$. The bold numbers 1 to 7 are the locations used in equations (2)–(8).

frequencies between 20–25 Hz. As the value is increased to 5, the lower limit of this subharmonic generation interval decreases to 10, making the interval wider as 10–25 Hz. It is important to note that ϕ_n^{stim} does not affect the alpha oscillation. Similar observations can be made for the parameter α. As α is varied from 50 to 200, the upper limit of the subharmonic frequency interval increases. However, with default values for other parameters alpha oscillation seems to cease as α is increased. With increasing α_{sr}, it can be deduced that the subharmonic region shifts upwards while its width stays unaffected. However, at higher values (e.g. 15 or 20), it seems that many complex nonlinear interactions occur, yielding a very crowded and unrealistic spectra. For ϕ_n^{BG}, lower values affect the presence of both alpha oscillation and subharmonic components while higher values yield complicated spectra with little effect on the subharmonic interval.

The observations we made from the effects of changing the 11 parameters individually, suggested us that the model is able to show very different subharmonic generation intervals for different parameter sets. We then proceeded to change the values of parameters simultaneously. Taking into consideration the individual effects of the parameters, we concluded not to include the input parameters ϕ_n^{stim} and ϕ_n^{BG} in this analysis because we believe that they do not reflect inherent properties of the visual system. Since we had observed that the effects of ν_{sr}, ν_{rs} and Q_{max} are weaker compared to the effects of other parameters, we neglected these parameters as well. Thus, we decided to only consider the six parameters (α, β, α_{sr}, β_{sr}, σ and θ) and keep ν_{sr}, ν_{rs}, Q_{max}, ϕ_n^{stim} and ϕ_n^{BG} unchanged from their values in table 1. In short, we searched for different subharmonic generation intervals by changing the values of the parameters α, β, α_{sr}, β_{sr}, σ and θ simultaneously.

Three examples of very different subharmonic generation intervals obtained after such analysis are given in figure 5. In the first plot, compared to the case with default parameter values, the subharmonic generation interval broadens to 15–30 Hz. We have also observed an entrainment behavior similar to the case with default parameter values (figure 3) except that the entrainment range seems to be 8–15 Hz and the native oscillation frequency is 13 Hz. In the second and third plots also, different ranges of subharmonic generation are observed with different parameter sets. However, the second and third plots also have some discrepancies conflicting with the entrainment theory as we discuss in the *Discussion* section.

3.4. Mechanism of PD generation within the intrathalamic loop

To further investigate the mechanism of subharmonic generation in the model, we isolated the intrathalamic

loop from the rest of the circuit (figure 6). The 'isolated' intrathalamic loop consists of two nonlinear elements (both of the shifted sigmoidal type), two gain elements and two second order low pass filters. For such feedback systems, it is known that constant amplitude oscillations occur if two conditions are satisfied at the frequency of interest: (i) loop gain should be unity (ii) total phase change across the loop should be 0 radians (or $2k\pi$ radians where $k = 0, 1, 2, \ldots$). Given that the system is driven with a signal of the form $DC + B\cos(\omega t + \phi)$, we may assume the following signal at location **1** (see bold numbers on figure 6) in the loop:

$$1: DC_1 + B_1\cos(\omega t + \phi_{B_1}) + A_1\cos\left(\frac{\omega}{2}t + \phi_{A_1}\right) \tag{2}$$

Here, the presence of $A_1\cos\left(\frac{\omega}{2}t + \phi_{A_1}\right)$ assumes that a subharmonic oscillation is obtained through the loop. We then need to relate the signal at location **1** to the one at location **2**. This is where describing function theory comes in handy, as it helps us to continue forming the loop equations as follows (also here we translate the signal to phasor representation, knowing that each component is at a different frequency). Below, each row of the vector corresponds to components at different frequencies (DC, stimulation frequency and subharmonic frequency from top to bottom):

$$2: \begin{bmatrix} DC_1N_1(0) \\ B_1e^{j\phi_{B1}}N_1(\omega) \\ A_1e^{j\phi_{A1}}N_1\left(\frac{\omega}{2}\right) \end{bmatrix} \tag{3}$$

Here N_1 stands for the describing function of the first nonlinear block in the loop. We then proceed with writing the signals at each location:

$$3: \begin{bmatrix} DC_1N_1(0)v_{rs} \\ B_1e^{j\phi_{B1}}N_1(\omega)v_{rs} \\ A_1e^{j\phi_{A1}}N_1\left(\frac{\omega}{2}\right)v_{rs} \end{bmatrix} \tag{4}$$

$$4: \begin{bmatrix} DC_1N_1(0)v_{rs}H_\alpha(0) \\ B_1e^{j\phi_{B_1}}N_1(\omega)v_{rs}H_\alpha(\omega) \\ A_1e^{j\phi_{A1}}N_1\left(\frac{w}{2}\right)v_{rs}H_\alpha\left(\frac{\omega}{2}\right) \end{bmatrix} \tag{5}$$

$$5: \begin{bmatrix} DC_1N_1(0)v_{rs}H_\alpha(0)N_2(0) \\ B_1e^{j\phi_{B_1}}N_1(\omega)v_{rs}H_\alpha(\omega)N_2(\omega) \\ A_1e^{j\phi_{A1}}N_1\left(\frac{w}{2}\right)v_{rs}H_\alpha\left(\frac{\omega}{2}\right)N_2\left(\frac{\omega}{2}\right) \end{bmatrix} \tag{6}$$

$$6: \begin{bmatrix} DC_1N_1(0)v_{rs}H_\alpha(0)N_2(0)v_{sr} \\ B_1e^{j\phi_{B_1}}N_1(\omega)v_{rs}H_\alpha(\omega)N_2(\omega)v_{sr} \\ A_1e^{j\phi_{A1}}N_1\left(\frac{\omega}{2}\right)v_{rs}H_\alpha\left(\frac{\omega}{2}\right)N_2\left(\frac{\omega}{2}\right)v_{sr} \end{bmatrix} \tag{7}$$

$$7: \begin{bmatrix} DC_1N_1(0)v_{rs}H_\alpha(0)N_2(0)v_{sr}H_{sr}(0) \\ B_1e^{j\phi_{B_1}}N_1(\omega)v_{rs}H_\alpha(\omega)N_2(\omega)v_{sr}H_{sr}(\omega) \\ A_1e^{j\phi_{A1}}N_1\left(\frac{\omega}{2}\right)v_{rs}H_\alpha\left(\frac{\omega}{2}\right)N_2\left(\frac{\omega}{2}\right)v_{sr}H_{sr}\left(\frac{\omega}{2}\right) \end{bmatrix} \tag{8}$$

Then we complete the loop (location **7** → location 1) and obtain 3 equation (2 are complex):

$$DC_1N_1(0)v_{rs}H_\alpha(0)N_2(0)v_{sr}H_{sr}(0) + DC = DC_1 \tag{9}$$

$$B_1e^{j\phi_{B_1}}N_1(\omega)v_{rs}H_\alpha(\omega)N_2(\omega)v_{sr}H_{sr}(\omega) + Be^{j\phi} = B_1e^{j\phi_{B1}} \tag{10}$$

$$A_1e^{j\phi_{A1}}N_1\left(\frac{\omega}{2}\right)v_{rs}H_\alpha\left(\frac{\omega}{2}\right)N_2\left(\frac{\omega}{2}\right)v_{sr}H_{sr}\left(\frac{\omega}{2}\right) = A_1e^{j\phi_{A1}} \tag{11}$$

For given DC, B, ϕ and ω, the above equation (5 real equations when the complex ones are separated as real and imaginary) can be solved for DC_1, A_1, B_1, ϕ_{A_1} and ϕ_{B_1}. The phase component ϕ can be selected arbitrarily as it only depends on the selection of the time origin. As shown in the second plot of figure 7 for a parameter set of $DC = 30$, $B = 2.8$, $\phi = 0$ and $\omega = 18$ Hz, we obtained $DC_1 = 456.6$, $A_1 = 360$, $B_1 = 215.5$. The significantly non-zero value of A_1 demonstrates that for the given input parameter set, a first subharmonic occurs. The first plot in figure 7 shows the results of simulation of the model shown in figure 6 for the same input parameter set. It is observed that using simulation, very close values for DC_1, A_1, B_1 were obtained. This means that, we are able to judge, without simulating the model, if a parameter set will generate subharmonic oscillations or not.

4. Discussion and conclusion

Period doubling in SSVEP experiments have been consistently observed across different studies [2, 6, 13–15]. The occurrence of period doubling has been speculated to be by 'entrainment' of intrinsic brain oscillations to half of the external stimulation frequency [14, 16, 17, 29]. Tsoneva *et al* define the term *entrainment* as the synchronization of naturally ongoing oscillations to an external force [14]. They have stated that the subharmonic components observed in their experiments, where they have used 40–60 Hz stimulation, are due to beta band (20–30 Hz) synchronization [14]. Similarly, Labecki *et al* describe *entrainment* as 'synchronization of two or more independent oscillators with differing natural frequencies, due to their coupling' [16]. In their study, they have applied periodic input to the neural mass model of Lopes da Silva *et al* [23] and have related subharmonic components to the entrainment of the resonant frequency of the model to half of the excitation frequency [16]. Roberts and Robinson

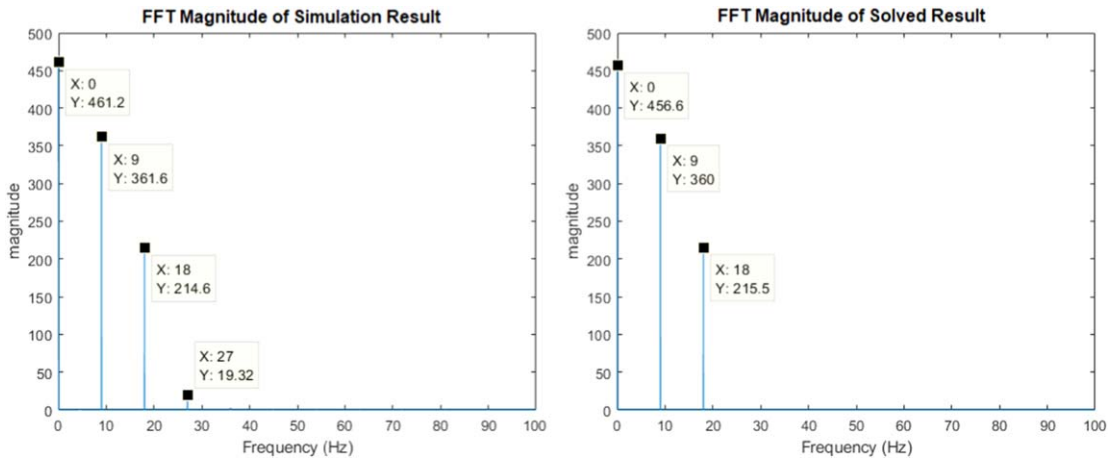

Figure 7. Plots showing compliance between simulation results and results from the equations. For any given DC, B, ϕ and ω, equations (9)–(11) (5 real equations when the complex ones are separated as real and imaginary) can be solved for the subharmonic magnitude and phase at any point in the loop. In this example the values are chosen as: $DC = 30$, $B = 2.8$, $\phi = 0$ and $\omega = 18Hz$. Notice that the effect of the 27 Hz (3 f /2) component is not considered while the equations were formed (due to sharp filtering characteristic of H_{sr}), hence the small differences between two results. Phases of the same components in the plots also show similar agreement (not shown here).

define this term as 'reduction of ongoing activity in favor of activity phase-locked to the drive, at frequencies harmonically related to the drive frequency' in their study where they have driven Robinson's corticothalamic model with periodic input [17]. They have stated that the alpha rhythm (the native oscillation of the model) is entrained to the drive frequency and its subharmonics [17]. However, these studies have not discussed the mechanism of entrainment. The closest mechanistic explanation of *entrainment* is given in the study of Notbohm *et al* [29]. They have devised a method to differentiate between whether an SSVEP is a superposition of event related potentials (i.e. superposition of the responses to each of the flashes of a square wave stimulation) or whether it is the entrainment of an intrinsic oscillator to the extrinsic driving stimulation. Comparing the phase synchrony between output and input for the cases of periodic stimulation and jittered periodic stimulation they have shown that SSVEPs are entrained-intrinsic oscillations if the driving source is strong and close in frequency. They have also shown that for relatively weak and relatively off-intrinsic-frequency excitation, the internal oscillator may slip at times and entrainment is not fully onset.

In this study, we have investigated the possible generation mechanism of the subharmonic oscillations using a corticothalamic model by Robinson [17, 20–22]. By scrutinizing the model, we have shown that the observed PD behavior has its origins at the intrathalamic feedback loop. Furthermore, we have determined, by nonlinear feedback theory, the conditions necessary for the occurrence of subharmonic oscillations, and thus have shed light to the mechanism of subharmonic generation. It may be asked if this mechanism is an explanation for a possible entrainment phenomenon. Although we do not refer to entrainment in explaining the mechanism of subharmonic generation, nevertheless we do not contradict with it when the end results are considered.

We have also observed that the model is able to show very different subharmonic generation intervals for different parameter sets (figures 3 and 5). However, this sometimes results in a different native oscillation frequency of the model. We predict that this shift is due to similar generation mechanisms between alpha and subharmonic oscillations, possibly in the intrathalamic loop.

Given our previous experimental results [15] shown in figure 1 and also Herrmann's experimental results [6], it is observed that if subharmonic frequency is near 8–15 Hz (i.e. when the stimulus frequency range is 15–30 Hz), alpha oscillation in the brain is facilitated towards this subharmonic frequency. When the stimulus frequency is outside the 15–30 Hz region, in our experimental studies, both alpha and subharmonic oscillations are observed which suggest that alpha entrainment does not occur and thus subharmonic generation has a different mechanism than alpha entrainment. However, in the simulations of the corticothalamic model, it is observed that when the subharmonic frequency is outside the alpha range, subharmonic oscillations cease to exist, and only alpha oscillations are observed. Thus, the model generates subharmonic oscillations only through the alleged 'alpha entrainment'.

We have also observed other discrepancies between model predictions and experimental results. As seen in the second plot of figure 5, as mentioned above, for a given parameter set, native oscillation frequency is increased together with the increase in the subharmonic oscillation range. However, in this case, the observed native oscillation frequency (18 Hz) is no longer in the human alpha rhythm range. In the third plot of figure 5, for a specific parameter set, we observed that the system showed PD behavior even

though it did not have any native oscillation. This contradicts with our previous observation that subharmonic oscillations are generated via entrainment of the alpha rhythm. We were not able to find a parameter set that would broaden the subharmonic region while keeping the native oscillation frequency in the normal human alpha rhythm range (native oscillations either shifted up above the human alpha rhythm range or totally vanished). To clarify the discrepancies between the model and the empirical observations, we think future intracranial recordings taken directly from subcortical structures under a periodic light stimulus will be instrumental.

In general, to further explore features of the PD generation by the corticothalamic model, a thorough parametric sweep study is necessary. However, such a study would be extremely memory and time consuming considering the number of parameters in the model and that a single simulation for a given parameter set takes 100 s in Simulink. We have provided a possible approach for speeding up such a sweep study by reducing the entire model to five nonlinear algebraic equations the solution of which shows whether subharmonic generation will occur or not. Therefore, instead of solving the system partial differential equations, which takes 100 s of simulation time with $dt = 10^{-4}$ s in Simulink for a given parameter set, these algebraic equations can be utilized as a fast semi-analytic parameter sweep modality. As a concluding remark, we strongly believe that subharmonic oscillations are important features of SSVEP responses, and that any modelling study regarding SSVEP responses should consider the presence of this empirically verified nonlinear behavior in the model output.

Acknowledgments

This work was supported by The Scientific and Technological Research Council of Turkey (TUBITAK) under Grant 116E153.

Appendix A

Seven subjects were presented a very accurate (nearly zero distortion) sinusoidal light emitted by two high gloss LEDs placed in a Do-It-Yourself cardboard Virtual Reality headset. The stimulation frequency range was 15–42 Hz, divided into two separate ranges, 15–32 and 28–42 Hz, for shorter sessions (so that experiments induce less visual fatigue). EEG was recorded at 1kS/s from six (O1, Oz, O2, Pz, P3, P4) electrodes all referenced to 'FCz'. A two dimensional plot was generated for better observation of the trends (fundamental, harmonic and subharmonic components) in the data. In this plot, the stimulation frequencies are placed on the horizontal axis and the power spectral density (PSD) estimate of the response to each stimulus frequency are grayscale coded on the vertical axis. More detailed explanations are available in the relevant paper [15].

Apart from statistical findings, we had observed subharmonic generation in the whole stimulus frequency range, 15–42 Hz. This is very clearly observable from the two dimensional plots generated for both 15–32 Hz and 28–42 Hz experiments (figure 1).

In both figures, lines on which the subharmonic components line up (labeled as 1:2 line in the figures) are clearly visible as well as the lines on which the fundamental and harmonic components reside (labeled as 1:1 and 2:1 lines respectively). A very important observation to make here is that subharmonic responses are more easily noticeable in the right-hand plot than in the left-hand plot in figure 1 because the subharmonic frequencies in the right-hand one do not fall in the alpha band.

Appendix B

Below we provide an explanation of the model formulations keeping the notation in the original work mostly unchanged [20–22].

In this model, each population is modeled by two main relations: (**i**) a linear operator $D_{ab} = \frac{1}{\alpha_{ab}\beta_{ab}}\frac{d^2}{dt^2} + \left(\frac{1}{\alpha_{ab}} + \frac{1}{\beta_{ab}}\right)\frac{d}{dt} + 1$ that relates the mean postsynaptic potential V_{ab} of population a to the mean afferent firing rate ϕ_b coming from the presynaptic population b by $D_{ab}V_{ab}(\boldsymbol{r}, t) = \nu_{ab}\phi_b(\boldsymbol{r}, t - \tau_{ab})$. Here ν_{ab} denotes the synaptic connection strength between populations a and b, τ_{ab} denotes the mean axonal delay between populations a and b and β_{ab}, α_{ab} denote the reciprocal rise and fall times of the membrane potential of population a due to input coming from population b, (**ii**) a nonlinear shifted sigmoidal function $Q_a = S[V_a] = \frac{Q_{\max}}{1 + \exp\left(-\frac{V_a - \theta}{\sigma}\right)}$ that relates the mean firing rate Q_a of population a to the same population's mean membrane potential $V_a = \sum_b V_{ab}$. Here, $Q_{\max}$ denotes the maximum firing rate, θ is the mean threshold voltage for the population and σ denotes the variance of this threshold value in the population.

Originally, the model regarded mean afferent firing rates ϕ_a as fields and these were governed by a damped wave equation with $Q_a = S[V_a]$ as the source:

$$\left[\frac{1}{\gamma_a^2}\frac{\partial^2}{\partial t^2} + \frac{2}{\gamma_a}\frac{\partial}{\partial t} + 1 - r_a^2\nabla^2\right]\phi_a(\boldsymbol{r}, t) = S[V_a(\boldsymbol{r}, t)] \tag{B.1}$$

where γ_a is the reciprocal delay due to axonal conduction and r_a is the axon length. However, in reducing the model to a neural mass model, we omitted the ∇^2 terms (since we assume there is no positional dependence in the cortex we also drop the **r** argument) for all populations $a = e, i, r, s$. For populations other than $a = e$ (i.e. for inhibitory interneurons and thalamic populations), axonal conduction delay $1/\gamma_a$ is taken to be zero, yielding

$$\phi_a(t) = S[V_a(t)] \tag{B.2}$$

for $a = i, r, s$

$$\left[\frac{1}{\gamma_a^2}\frac{d^2}{dt^2} + \frac{2}{\gamma_a}\frac{d}{dt} + 1\right]\phi_a(t) = S[V_a(t)] \tag{B.3}$$

for $a = e$.

Note that the operator in 2.3 is different from the two main relations explained above. Specifically, this does not convert firing rate to potential or vice versa, it is only introducing a delay to the excitatory population dynamics due to longer ranged axonal connections of the excitatory neurons.

The authors made further assumptions regarding intrathalamic and intracortical connectivities [17]: they took all $\beta_{ab} = \beta$, $\alpha_{ab} = \alpha$ (hence $D_{ab} = D_\alpha$ except for the intrathalamic β_{sr} and α_{sr} values (hence $D_{sr} \neq D_\alpha$) due to slower dynamics, and they took $V_e = V_i$ due to random intracortical connectivity.

Given above assumptions and derivations, the model equations are:

Contribution by firing rate coming from sensory population (ϕ_n) to mean membrane potential of thalamic relay population V_{sn}:

$$D_\alpha V_{sn}(t) = \nu_{sn}\phi_n(t) \tag{B.4}$$

Contribution by firing rate coming from thalamic reticular cell population (ϕ_r) to mean membrane potential of thalamic relay population V_{sr}:

$$D_{sr} V_{sr}(t) = \nu_{sr}\phi_r(t) \tag{B.5}$$

Contribution by firing rate coming from excitatory cortical interneurons (ϕ_e) to mean membrane potential of thalamic relay population V_{se}:

$$D_\alpha V_{se}(t) = \nu_{se}\phi_e\left(t - \frac{t_0}{2}\right) \tag{B.6}$$

Mean membrane potential of thalamic relay population V_s:

$$V_s(t) = V_{sn}(t) + V_{sr}(t) + V_{se}(t) \tag{B.7}$$

Contribution by firing rate coming from excitatory cortical interneurons (ϕ_e) to mean membrane potential of thalamic reticular population V_{re}:

$$D_\alpha V_{re}(t) = \nu_{re}\phi_e\left(t - \frac{t_0}{2}\right) \tag{B.8}$$

Contribution by firing rate coming from thalamic relay cell population (ϕ_s) to mean membrane potential of thalamic reticular population V_{rs}:

$$D_\alpha V_{rs}(t) = \nu_{rs}\phi_s(t) \tag{B.9}$$

Mean membrane potential of thalamic reticular population V_r:

$$V_r(t) = V_{re}(t) + V_{rs}(t) \tag{B.10}$$

Contribution by firing rate coming from excitatory cortical interneurons (ϕ_e) to mean membrane potential of excitatory cortical interneuron population V_{ee}:

$$D_\alpha V_{ee}(t) = \nu_{ee}\phi_e(t) \tag{B.11}$$

Contribution by firing rate coming from inhibitory cortical interneurons (ϕ_i) to mean membrane potential of excitatory cortical interneuron population V_{ei}:

$$D_\alpha V_{ei}(t) = \nu_{ei}\phi_i(t) \tag{B.12}$$

Contribution by firing rate coming from thalamic relay cell population (ϕ_s) to mean membrane potential of excitatory cortical interneuron population V_{es}:

$$D_\alpha V_{es}(t) = \nu_{es}\phi_s\left(t - \frac{t_0}{2}\right) \tag{B.13}$$

Mean membrane potential of excitatory cortical interneuron population V_e:

$$V_e(t) = V_{ee}(t) + V_{ei}(t) + V_{es}(t) \tag{B.14}$$

Mean afferent firing rate ϕ_s of the thalamic relay population with a mean membrane potential of V_s:

$$\phi_s = S[V_s(t)] \tag{B.15}$$

Mean afferent firing rate ϕ_r of the thalamic reticular population with a mean membrane potential of V_r:

$$\phi_r = S[V_r(t)] \tag{B.16}$$

Mean afferent firing rate ϕ_i of the inhibitory cortical interneuron population with a mean membrane potential of $V_i = V_e$:

$$\phi_i = S[V_i(t)] = S[V_e(t)] \tag{B.17}$$

Mean afferent firing rate ϕ_e of the excitatory cortical interneuron population with a mean membrane potential of V_e:

$$\left[\frac{1}{\gamma_e^2}\frac{d^2}{dt^2} + \left(\frac{2}{\gamma_e}\right)\frac{d}{dt} + 1\right]\phi_e(t) = S[V_e(t)] \tag{B.18}$$

Appendix C

In figure C1, effects of the remaining seven (ν_{sr}, ν_{rs}, β, β_{sr}, Q_{max}, σ, θ) different parameters on subharmonic generation are shown. In all these plots, default values are used for parameters other than the swept parameter. As β is increased from 150 to 2000, subharmonic regime tends to slowly shift from 10–20 Hz to 15–25 Hz, keeping its width pretty much unchanged. The alpha oscillation frequency shifts from ~8 Hz to ~12 Hz as β is increased (power at alpha components seems to drop as is β increased). For lower values of β, the spectrum becomes very crowded and complex possibly owing to many nonlinear interactions taking effect. For values $\beta > 800$, the spectrum remains largely unaffected (only change seems to be the decreasing power at alpha band) from increasing β. As β_{sr} is varied from 10 to 200, the subharmonic regime shifts upwards (i.e. 5–15 Hz to 25–35 Hz) with decreasing power at this regime (at $\beta_{sr} = 200$, the subharmonic components are barely distinguishable from background). The native oscillation frequency (f_α) also shifts upwards with the

subharmonic regime, going outside the alpha band. The effects of increasing $Q_{\max}$ is not as impactful as other parameters. The position of the subharmonic regime is unaffected, while its width is barely affected at the upper limit (the interval changed from 15–24 Hz to 15–25 Hz). The power of the alpha oscillation seems to increase as $Q_{\max}$ increases with its frequency fairly unaffected. σ is arguably the most influential parameter on the subharmonic regime. For lower values ($\sigma = 2, 2.5$) , the spectrum is utterly cluttered, with lots of nonlinear components including many higher order subharmonics. For higher values of σ, both the subharmonic regime and alpha oscillation vanish, only leaving the fundamental and harmonic components in the spectrum. θ significantly affects the width of the subharmonic regime. As it is varied from 10 to 25, subharmonic regime first extends from the upper limit then from the lower limit (at $\theta = 20$ the width is doubled). After $\theta = 20$, the regime tends to shift downwards with vanishing power at alpha oscillation. For $\nu_{rs} = 0.2$, subharmonic regime is inexistent. For increasing ν_{rs} values, the width of the regime is subtly affected at the upper limit, but the alpha oscillation frequency shifts upwards, from ∼10 Hz to ∼12 Hz. Higher values for ν_{sr}, kill off both the subharmonic components and the alpha oscillation (as expected due to negative feedback). At lower values, subharmonic regime seems to be faintly affected by ν_{sr} while alpha oscillation seems to cease as ν_{sr} is increased from 0.2 to 1.5.

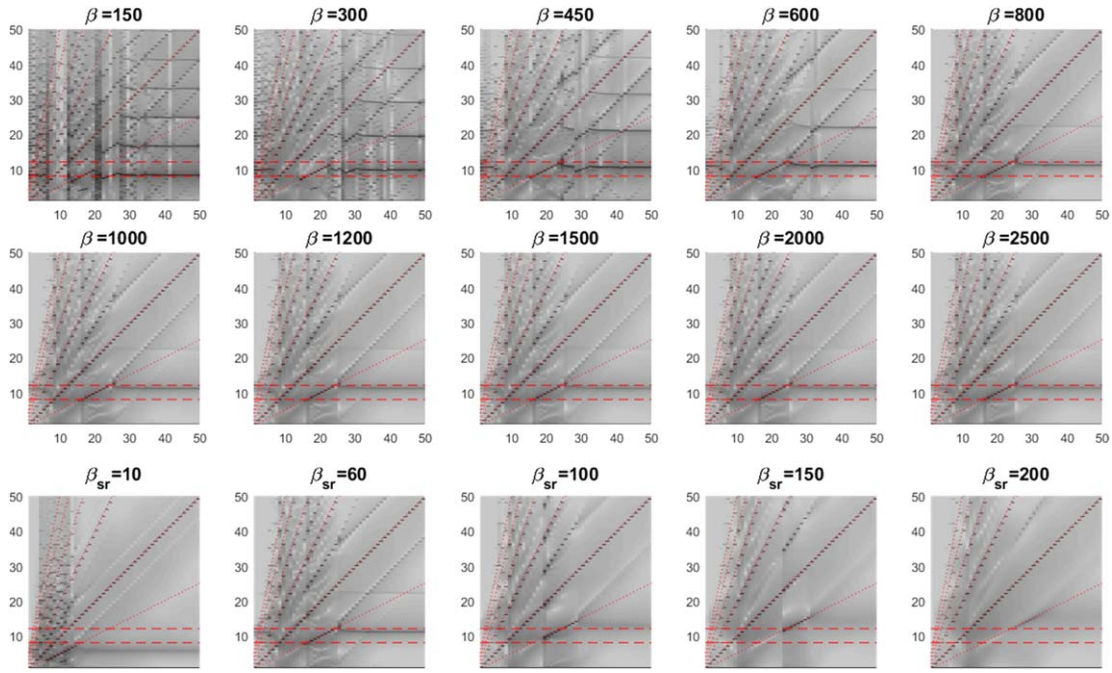

Figure C1. Effects of seven (ν_{sr}, ν_{rs}, β, β_{sr}, Q_{max}, σ, θ) different parameters on subharmonic generation are shown. In these plots, the stimulation frequencies are placed on the horizontal axis and the PSD estimate of the response to each stimulus frequency is grayscale coded on the vertical axis. Two topmost rows show model responses for $\beta = 150, 300, 450, 600, 800, 1000, 1200, 1500, 2000, 2500$ third row for $\beta_{sr} = 10, 60, 100, 150, 200$, fourth row for $Q_{max} = 100, 200, 250, 300, 400$, fifth row for $\sigma = 2,\ 2.5,\ 3.3,\ 4,\ 5$, fifth row for $\theta = 10, 15, 20, 25$, sixth row for $\nu_{rs} = 0.2, 0.6, 1.5, 2.9, 4$, and bottommost row for $\nu_{sr} = 0.2, 0.57, 1.5, 3, 5$. While these values are swept for the relevant parameter, the values for other parameters are selected as in table 1.

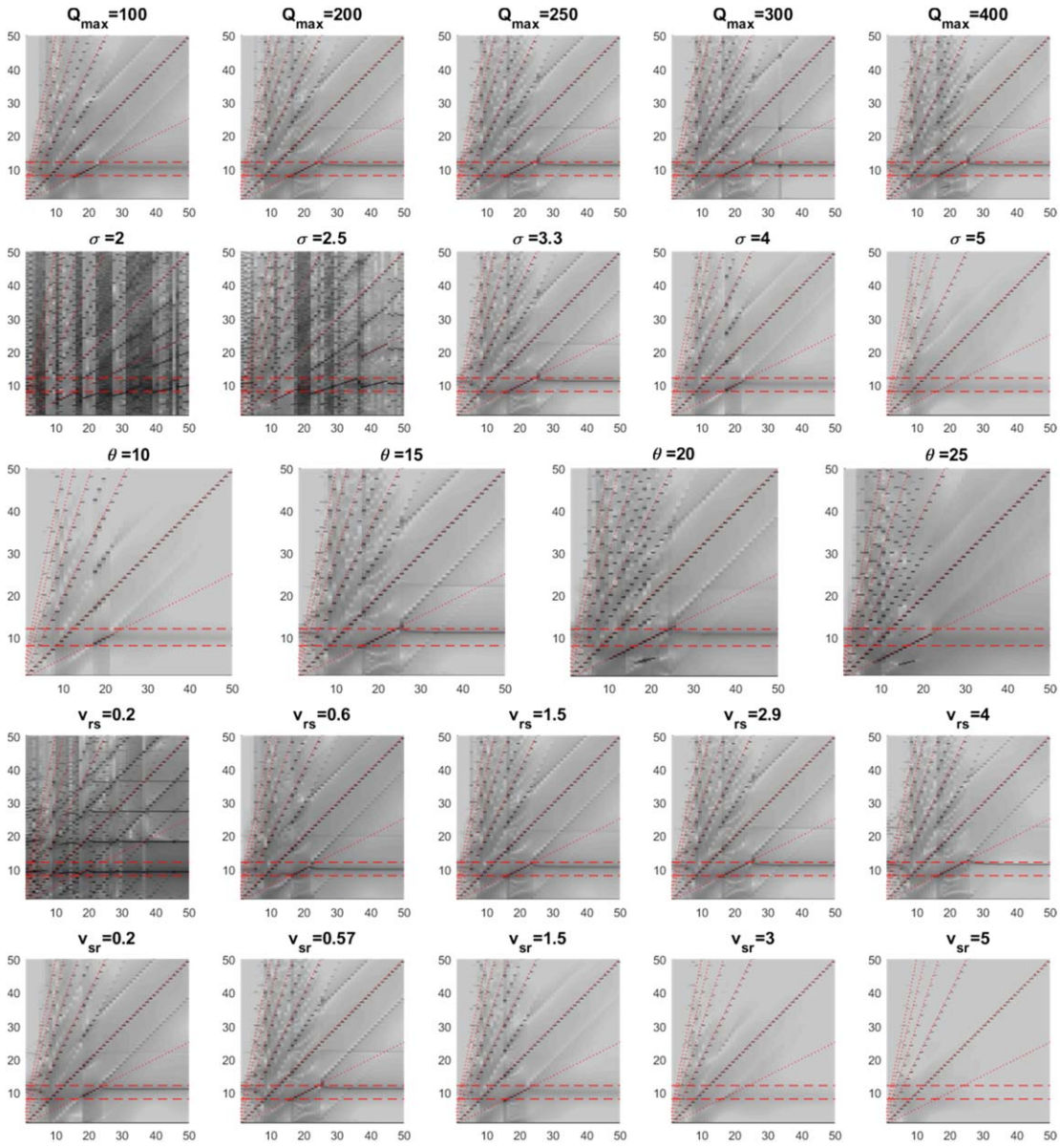

Figure C1. (Continued.)

ORCID iDs

Yiğit Tuncel https://orcid.org/0000-0001-5943-0230
Toygun Başaklar https://orcid.org/0000-0002-9312-236X
Yusuf Ziya Ider https://orcid.org/0000-0002-1961-6804

References

[1] Regan D 1966 Some characteristics of average steady-state and transient responses evoked by modulated light *Electroencephalogr. Clin. Neurophysiol.* **20** 238–48
[2] Regan D 1989 *Human Brain Electrophysiology: Evoked Potentials and Evoked Magnetic Fields in Science and Medicine* (New York: Elsevier)
[3] Yin E, Zhou Z, Jiang J, Yu Y and Hu D 2015 A dynamically optimized SSVEP brain–computer interface (BCI) Speller *IEEE Trans. Biomed. Eng.* **62** 1447–56
[4] Yin E, Zeyl T, Saab R, Chau T, Hu D and Zhou Z 2015 A hybrid brain–computer interface based on the fusion of P300 and SSVEP scores *IEEE Trans. Neural Syst. Rehabil. Eng.* **23** 693–701
[5] Zhang Y, Yin E, Li F, Zhang Y, Tanaka T, Zhao Q, Cui Y, Xu P, Yao D and Guo D 2018 Two-stage frequency recognition method based on correlated component analysis for SSVEP-based BCI *IEEE Trans. Neural Syst. Rehabil. Eng.* **26** 1314–23
[6] Herrmann C S 2001 Human EEG responses to 1–100 Hz flicker: resonance phenomena in visual cortex and their potential correlation to cognitive phenomena *Experimental Brain Research* **137** 346–53
[7] Nunez P L and Cutillo B A 1995 *Neocortical Dynamics and Human EEG Rhythms* (New York: Oxford University Press)
[8] Vialatte F-B, Maurice M, Dauwels J and Cichocki A 2010 Steady-state visually evoked potentials: Focus on essential paradigms and future perspectives *Prog. Neurobiol.* **90** 418–38
[9] Norcia A M, Appelbaum L G, Ales J M, Cottereau B R and Rossion B 2015 The steady-state visual evoked potential in vision research: a review *Journal of Vision* **15** 4

[10] Rager G and Singer W 1998 The response of cat visual cortex to flicker stimuli of variable frequency *European Journal of Neuroscience* **10** 1856–77
[11] Tweel L H and Spekreijse H 1969 Signal transport and rectification in the human evoked-response system *Ann. N.Y. Acad. Sci.* **156** 678–95
[12] Townsend R, Lubin A and Naitoh P 1975 Stabilization of alpha frequency by sinusoidally modulated light *Electroencephalogr. Clin. Neurophysiol.* **39** 515–8
[13] Crevier D W and Markus M 1998 Synchronous period-doubling in flicker vision of salamander and man *J. Neurophysiol.* **79** 1869–78
[14] Tsoneva T, Garcia-Molina G and Desain P 2015 Neural dynamics during repetitive visual stimulation *J. Neural Eng.* **12** 066017
[15] Tuncel Y, Başaklar T and Ider Y Z 2018 Period doubling behavior in human steady state visual evoked potentials *Biomedical Physics & Engineering Express* **4** 025024
[16] Labecki M, Kus R, Brzozowska A, Stacewicz T, Bhattacharya B S and Suffczynski P 2016 Nonlinear origin of SSVEP spectra a combined experimental and modeling study *Front. Comput. Neurosci.* **10** 129
[17] Roberts J A and Robinson P A 2012 Quantitative theory of driven nonlinear brain dynamics *NeuroImage* **62** 1947–55
[18] Spiegler A 2011 *Dynamics of Biologically Informed Neural Mass Models of The Brain* (Ilmenau: Univ.-Verl.)
[19] Jansen B H and Rit V G 1995 Electroencephalogram and visual evoked potential generation in a mathematical model of coupled cortical columns *Biol. Cybern.* **73** 357–66
[20] Robinson P A, Loxley P N, O'Connor S C and Rennie C J 2001 Modal analysis of corticothalamic dynamics, electroencephalographic spectra, and evoked potentials *Phys. Rev.* E **63** 041909
[21] Robinson P A, Rennie C J and Rowe D L 2002 Dynamics of large-scale brain activity in normal arousal states and epileptic seizures *Phys. Rev.* E **65** 041924
[22] Rennie C J, Robinson P A and Wright J J 2002 Unified neurophysical model of EEG spectra and evoked potentials *Biol. Cybern.* **86** 457–71
[23] Lopes da Silva F H, Hoeks A, Smits H and Zetterberg L H 1974 Model of brain rhythmic activity *Kybernetik* **15** 27–37
[24] Lopes da Silva F H and Leeuwen W S V 1977 The cortical source of the alpha rhythm *Neurosci. Lett.* **6** 237–41
[25] Robinson P, Rennie C, Rowe D and Oconnor S 2004 Estimation of multiscale neurophysiologic parameters by electroencephalographic means *Human Brain Mapping* **23** 53–72
[26] Breakspear M, Roberts J A, Terry J R, Rodrigues S, Mahant N and Robinson P A 2005 A unifying explanation of primary generalized seizures through nonlinear brain modeling and bifurcation analysis *Cerebral Cortex* **16** 1296–313
[27] West J C and Douce J L 1955 The mechanism of sub-harmonic generation in a feedback system *Proceedings of the IEE - Part B: Radio and Electronic Engineering* **102** 569–74
[28] Gelb A and Earl V V W 1968 *Multiple-Input Describing Functions and Nonlinear System Design* (New York: McGraw-Hill)
[29] Notbohm A, Kurths J and Herrmann C S 2016 Modification of brain oscillations via rhythmic light stimulation provides evidence for entrainment but not for superposition of event-related responses *Frontiers in Human Neuroscience* **10**